



# Exploring the Molecular Basis for Substrate Affinity and Structural Stability in Bacterial GH39 $\beta$ -Xylosidases

## OPEN ACCESS

### Edited by:

Fu-Li Li,  
Qingdao Institute of Bioenergy and  
Bioprocess Technology (CAS), China

### Reviewed by:

Yejun Han,  
University of the Chinese Academy  
of Sciences, China  
Md. Abu Saleh,  
University of Rajshahi, Bangladesh  
Ming Lu,  
Institute of Bioenergy and Bioprocess  
Technology (CAS), China

### \*Correspondence:

Mário Tyago Murakami  
mario.murakami@lnbr.cnpem.br;  
mario.t.murakami@gmail.com

† These authors have contributed  
equally to this work

### Specialty section:

This article was submitted to  
Bioprocess Engineering,  
a section of the journal  
Frontiers in Bioengineering and  
Biotechnology

Received: 28 February 2020

Accepted: 14 April 2020

Published: 15 May 2020

### Citation:

Morais MABd, Polo CC,  
Domingues MN, Persinoti GF,  
Pirolla RAS, de Souza FHM,  
Correa JBdL, dos Santos CR and  
Murakami MT (2020) Exploring  
the Molecular Basis for Substrate  
Affinity and Structural Stability  
in Bacterial GH39  $\beta$ -Xylosidases.  
*Front. Bioeng. Biotechnol.* 8:419.  
doi: 10.3389/fbioe.2020.00419

Mariana Abrahão Bueno de Morais<sup>1†</sup>, Carla Cristina Polo<sup>2†</sup>,  
Mariane Noronha Domingues<sup>1</sup>, Gabriela Felix Persinoti<sup>1</sup>,  
Renan Augusto Siqueira Pirolla<sup>1</sup>, Flávio Henrique Moreira de Souza<sup>1</sup>,  
Jessica Batista de Lima Correa<sup>1</sup>, Camila Ramos dos Santos<sup>1</sup> and  
Mário Tyago Murakami<sup>1\*</sup>

<sup>1</sup> Brazilian Biorenewables National Laboratory, Brazilian Center for Research in Energy and Materials, Campinas, Brazil,

<sup>2</sup> Brazilian Synchrotron Light Laboratory, Brazilian Center for Research in Energy and Materials, Campinas, Brazil

The glycoside hydrolase family 39 (GH39) is a functionally expanding family with limited understanding about the molecular basis for substrate specificity and extremophilicity. In this work, we demonstrate the key role of the positive-subsite region in modulating substrate affinity and how the lack of a C-terminal extension impacts on oligomerization and structural stability of some GH39 members. The crystallographic and SAXS structures of a new GH39 member from the phytopathogen *Xanthomonas citri* support the importance of an extended C-terminal to promote oligomerization as a molecular strategy to enhance thermal stability. Comparative structural analysis along with site-directed mutagenesis showed that two residues located at the positive-subsite region, Lys166 and Asp167, are critical to substrate affinity and catalytic performance, by inducing local changes in the active site for substrate binding. These findings expand the molecular understanding of the mechanisms involved in substrate recognition and structural stability of the GH39 family, which might be instrumental for biological insights, rational enzyme engineering and utilization in biorefineries.

**Keywords:** glycoside hydrolase family 39, structural stability, substrate specificity, X-ray crystallography, *Xanthomonas citri*

## INTRODUCTION

Bacterial glycoside hydrolase family 39 (GH39) members typically act as  $\beta$ -xylosidases (Vocadlo et al., 2002; Czjzek et al., 2005; Corrêa et al., 2012), but recent studies have shown that some GH39 enzymes can be devoid of catalytic activity against small xylose-based substrates (Ali-Ahmad et al., 2017). Instead, such enzymes are polyspecific (Jones et al., 2017) and involved in biofilm formation (Baker et al., 2015). These findings demonstrate a more diverse functional role of bacterial GH39 members than previously envisaged and open new questions regarding the molecular basis for substrate specificity in this family. Moreover, the existence of few GH39 structurally characterized

members in CAZy database (Lombard et al., 2014) reveals that this family is still poorly explored and mechanistic details for substrate binding remain mostly unknown.

By elucidating the crystal structure of the mesophilic GH39 enzyme from the oligotrophic bacterium *Caulobacter crescentus* (Santos et al., 2012), it was verified a C-terminal shortening in comparison to thermophilic GH39 members (Yang et al., 2004; Czjzek et al., 2005), which precluded the formation of tetramers. However, the scarce in solution and structural information for other members of the family remained inconclusive whether there is a correlation between the C-terminal extension and extremophilicity.

The plant pathogen bacterium *Xanthomonas citri* is the causative agent of the citrus canker and contains a broad arsenal of glycoside hydrolases for hemicellulose degradation including endo- $\beta$ -1,4-xylosidases,  $\beta$ -xylosidases, arabinofuranosidases, acetyl xylan esterases, and  $\alpha$ -glucuronidases. Besides being of industrial interest, these enzymes play important roles in virulence and survival of *Xanthomonas* species (Rajeshwari et al., 2005; Szczesny et al., 2010; Déjean et al., 2013). Among these enzymes the XacXynB, a putative  $\beta$ -xylosidase belonging to GH39, was found in the genome of *X. citri* (Silva et al., 2002) and according to its primary sequence it presents the C-terminal shortening as observed to *C. crescentus*, CcXynB2 (Santos et al., 2012).

Herein, we describe the structural and functional characterization of the GH39 XacXynB, contributing with new structural determinants for substrate recognition in its family, based on site-directed mutagenesis and molecular dynamics simulations, and supporting a role of the extended C-terminus in extremophilicity, combining phylogenetic analysis with high resolution structure determination.

## MATERIALS AND METHODS

### Molecular Cloning and Site-Directed Mutagenesis

XacXynB gene (GenBank: AAM38893.1) from *X. citri* codifies a 502 amino-acid residues mature protein with homology to the GH39 family. The signal peptide was removed and a 6xHis-tag was inserted, using the pET28a vector aiming further purification steps. The mutants K166D and D167G were generated by site-directed mutagenesis. The amount of 30  $\mu$ mol of the designed primers (K166D\_R: 5' gcggtctcccagaatcatcagattgggctcgttc and K166D\_F: 5' ggaacgagcccaatctggatgatttctgggagaacgc; D167G\_R: 5' cggcgttctcccagaacccttcagattgggctc and D167G\_F: 5' gagcccaatctgaaggggttctgggagaacgcgc) were added to 20.8 ng  $\cdot$   $\mu$ L<sup>-1</sup> of pET28a-XacXynB with 0.5 mM dNTPs, 1  $\mu$ M Mg(SO<sub>4</sub>)<sub>2</sub>, 5  $\mu$ L Platinum<sup>®</sup> Pfx DNA Polymerase 10 $\times$  buffer and 1.25 U Platinum<sup>®</sup> Pfx DNA Polymerase (Life Technologies, Carlsbad, CA, United States). The annealing and extension temperatures were 55°C during 60 s and 68°C for 7 min, respectively. The procedure was repeated by 18 cycles. In order to digest methylated parental DNA, the reaction was incubated with 1 U *Dpn*I (Fermentas, Waltham, MA, United States), 37°C during 1 h. The reaction product was transformed into competent *Escherichia coli* DH5 $\alpha$  cells and

after growing, plated into 2% (*v/w*) Luria-Bertani containing 50  $\mu$ g  $\cdot$  mL<sup>-1</sup> kanamycin and 50  $\mu$ g  $\cdot$  mL<sup>-1</sup> chloramphenicol. After 16 h growing at 37°C, the clones DNA were extracted and submitted to Sanger sequencing.

### Protein Expression and Lysis

All plasmids were transformed into thermocompetent BL21(DE3) $\Delta$ SlyD cells with pRARE2 plasmid and grown in LB containing 2% (*v/v*) of inoculum, 50  $\mu$ g  $\cdot$  mL<sup>-1</sup> kanamycin and 50  $\mu$ g  $\cdot$  mL<sup>-1</sup> chloramphenicol at 37°C, 4 h at 200 rpm until A<sub>600 nm</sub> reached 0.7. The induction with 0.1 mM Isopropyl  $\beta$ -D-1-thiogalactopyranoside was performed at 20°C for 16 h. The cells were collected by harvesting at 5000  $\times$  g and resuspended in lysis buffer (20 mM sodium phosphate, pH 7.5, 500 mM NaCl, 5 mM imidazole, 1 mM phenylmethylsulfonyl fluoride and 5 mM benzamidine), and disrupted by lysozyme treatment (80  $\mu$ g  $\cdot$  mL<sup>-1</sup>, 30 min, on ice), followed by sonication (50% amplitude and 6 pulses of 15 s on ice using a tip 406) in a Vibracell VCX 500 device (Sonics and Materials, Newtown, CT, United States). The extract was harvested at 30,000  $\times$  g and filtered.

### Purification Steps

All purification steps were performed using a Fast Performance Liquid Chromatography System (GE Healthcare, Little Chalfont, United Kingdom). The crude extract was applied, at 1 mL  $\cdot$  min<sup>-1</sup> flow rate, into a 5 mL HiTrap Chelating column (GE Healthcare, Little Chalfont, United Kingdom) charged with 100 mM NiSO<sub>4</sub> and pre-equilibrated with 20 mM sodium phosphate, pH 7.5, 500 mM NaCl and 5 mM imidazole. The extract was washed with 10 column volumes and eluted in a 0–100% non-linear gradient with a buffer containing 500 mM imidazole. The following step of size-exclusion chromatography was performed in a HiLoad Superdex 75 16/60 column (GE Healthcare, Little Chalfont, United Kingdom) pre-equilibrated with 20 mM sodium phosphate, pH 7.5, 150 mM NaCl with a 0.5 mL  $\cdot$  min<sup>-1</sup> flow rate.

### Circular Dichroism

A purified XacXynB sample was analyzed by far-UV circular dichroism (CD) measurements (195–260 nm), at a protein concentration of 0.2 mg  $\cdot$  mL<sup>-1</sup> in 20 mM of sodium phosphate pH 7.4. CD measurements were carried out using a JASCO 815 spectropolarimeter (JASCO Inc., Tokyo, Japan) equipped with a Peltier temperature control unit using a 0.1 cm path quartz cuvette. The solvent spectra were subtracted in all experiments to eliminate background effects. The CD spectrum was the average of 20 accumulations using a scanning speed of 100 nm  $\cdot$  min<sup>-1</sup>, spectral bandwidth of 1 nm, and response time of 0.5 s. The thermal denaturation of the enzyme was characterized by measuring the ellipticity changes at 222 nm induced by a temperature increase from 20 to 100°C, at a heating rate of 1°C  $\cdot$  min<sup>-1</sup>.

### Crystallization

Crystallization experiments were carried out using the sitting-drop vapor-diffusion method. For initial screening, 0.5  $\mu$ L of the

protein solution at a concentration of 30 mg·mL<sup>-1</sup> in 20 mM Tris-HCl (pH 7.5, 150 mM NaCl) was mixed with an equal volume of the screening solution and equilibrated against a reservoir containing 80  $\mu$ L of the latter solution at 18°C. Single crystals appeared in a condition consisting of 0.1 M MIB Buffer (pH 5.0) and 25% (w/v) PEG1500 after 5 days.

## X-Ray Diffraction Data Collection and Processing

Crystals were transferred into a cryosolution consisting of the reservoir solution supplemented with 20% (v/v) glycerol and were flash-cooled in a nitrogen-gas stream at 100 K for data collection. X-ray diffraction data were collected at the MX2 beamline (LNLS, Campinas, Brazil) with the radiation wavelength set to 1.459 Å. The images were collected using an oscillation angle of 1° and an exposure time of 30 s per image. The MAR Mosaic 225 mm (MAR Research, Norderstedt, Germany) charge-coupled device (CCD) was used to record the intensities. Data were processed using the XDS package (Kabsch, 2010).

## Structure Determination and Refinement

The crystal structure of XacXynB was solved by molecular replacement (MR) calculations through the program PHASER (McCoy et al., 2007) using CcXynB (PDB entry: 4EKJ) as template. The best MR solution required extensive manual chain tracing, mainly of the C-terminal subdomain. Refinement cycles were carried out with REFMAC5 (Murshudov et al., 1997) or PHENIX refine (Afonine et al., 2012). After each cycle of refinement, the model was inspected and manually adjusted to correspond to computed  $\sigma_A$ -weighted ( $2F_o - F_c$ ) and ( $F_o - F_c$ ) electron density maps using the program COOT (Emsley and Cowtan, 2004). The water molecules were manually added at positive peaks above 2.0  $\sigma$  in the difference Fourier maps, taking into consideration hydrogen-bonding distances. The refined structure was evaluated using the program MolProbity (Chen et al., 2010).

## Small Angle X-Ray Scattering

SAXS measurements were performed at the SAXS1 beamline (LNLS, Campinas, Brazil). The radiation wavelength was set to 1.488 Å and X-ray scattering was recorded using a Pilatus 300 K (Dectris, Baden, Switzerland). The sample-to-detector distance was adjusted to a scattering-vector range of  $0.01 < q < 0.25 \text{ \AA}^{-1}$ , where  $q$  is the magnitude of the  $q$ -vector defined by  $q = 4\pi \sin\theta/\lambda$  ( $2\theta$  is the scattering angle). 10 frames of 30 s each were recorded to monitor radiation damage. Buffer scattering was recorded and was subtracted from the protein scattering. The integration of SAXS patterns was performed using FIT2D (Hammersley et al., 1997). Data were analyzed using the GNOM program (Svergun, 1992). The radius of gyration ( $R_g$ ) was estimated by the indirect Fourier transform method and the distance distribution function  $P(r)$  was calculated from the scattering curve using the maximum diameter ( $D_{\max}$ ) as a parameter. The molecular envelopes were calculated from the experimental SAXS data using the program DAMMIN (Svergun, 1999). Ten runs of *ab initio* shape determination yielded highly similar models

[normalized spatial discrepancy (NSD) values of  $<1$ ], which were then averaged using the DAMAVER package (Volkov and Svergun, 2003). The crystallographic structure was fitted into the SAXS molecular envelope using the program SUPCOMB (Kozin and Svergun, 2001).

## Phylogenetic Analysis

The full-length sequences of characterized GH39 enzymes described in CAZy database were retrieved along with XacXynB. A multiple sequence alignment was performed using MAFFT v7.299b (Katoh et al., 2002) and a Maximum Likelihood phylogenetic tree based on the WAG matrix-based model was constructed using FastTree v2.1.8 software (Price et al., 2010). The phylogenetic tree was visualized and annotated using the iTol web tool.

## Enzyme Assays

XacXynB (WT and mutants) was incubated with 2 mM of 4-nitrophenyl  $\beta$ -D-xylopyranoside (Sigma-Aldrich, St. Louis, MO, United States) and the product release was quantified at 400 nm. To determine the optimum pH and temperature profiles, enzymatic reactions were carried out at different pHs using McIlvaine (McIlvaine, 1921) buffers (pH 3.5–8.0, with 0.5 steps) and at a temperature range of 15–75°C (with 5°C steps). The absorbance values were converted in relative activity. These assays were performed in triplicate. Kinetic characterization was performed in a substrate range of 0.1–25 mM (4-nitrophenyl  $\beta$ -D-xylopyranoside), 50 mM McIlvaine buffer pH 5.5 (McIlvaine, 1921), with 13.6  $\mu$ M of enzyme at 40°C during 15 min. Kinetic parameters,  $K_M$ ,  $V_{\max}$ ,  $k_{\text{cat}}$ , and  $k_{\text{cat}}/K_M$ , were calculated from initial velocities.

## Capillary Zone Electrophoresis

The cleavage of xylooligosaccharides (XOS) from xylobiose (X2) to xylohexaose (X6) was analyzed at pH 5.5 at 40°C. Aliquots were taken after 16 h of reaction and heated to 95°C for 15 min for enzyme inactivation. For labeling, samples were incubated with 20  $\mu$ L  $\mu$ M citric acid (2.5 M), 8  $\mu$ L sodium cyanoborohydride (1 M) and 1.5  $\mu$ L APTS (100 mM). The samples were incubated at 80°C for 2 h, dried and then resuspended in 90  $\mu$ L of running buffer (40 mM potassium phosphate pH 2.5). The derivatized sugars were analyzed in a P/ACE MDQ instrument (Beckman Coulter, Brea, CA, United States) equipped with a laser induced fluorescence detection module. A capillary of 50  $\mu$ m internal diameter and 20 cm effective length was used. Electrophoretic conditions were set to 20 kV/70–100 mA with reverse polarity at 25°C. APTS-labeled sugars were excited at 488 nm and emission was detected at 520 nm. The electrophoretic behavior of labeled products was compared to standards.

## Molecular Dynamics Simulations

Molecular dynamics simulations were performed with WT XacXynB, and K166D and D167G mutants. Mutations were introduced manually by replacement of the residues from WT crystal structure before simulations. A His-tag fragment

(present in the crystal structure) from residues Gly-5 to His2 was removed prior to the simulations. The protonation state of all residues was assigned considering neutral pH. Protonation of His residues were further assessed according to their chemical environment. The inferred acid/base residue (Glu162) was protonated since its pKa was approximately 9 according to the program PROPKA (Li et al., 2005). Simulations were performed using Amber18 software (Case et al., 2018) with the FF14SB force-field (Maier et al., 2015) for the protein and the TIP3P force-field (Jorgensen et al., 1983) for water molecules. The systems were minimized, keeping the protein fixed and then the entire systems have been allowed to relax. The systems were heated in steps (to 100, 200, and 300 K) in the NVT ensemble at intervals of 50 ps. Spatial restraints were applied to the entire protein during the first heating interval (to 100 K), being all restraints released after this step. The density was converged up to water density at 300 K during 100 ps in the NPT ensemble. Runs of 100 ps were performed to equilibrate the root-mean-square deviation (RMSD) in the NVT ensemble with a time step of 1 fs. The time step was subsequently increased to 2 fs, employing the SHAKE algorithm (Ryckaert et al., 1977). Simulations have been

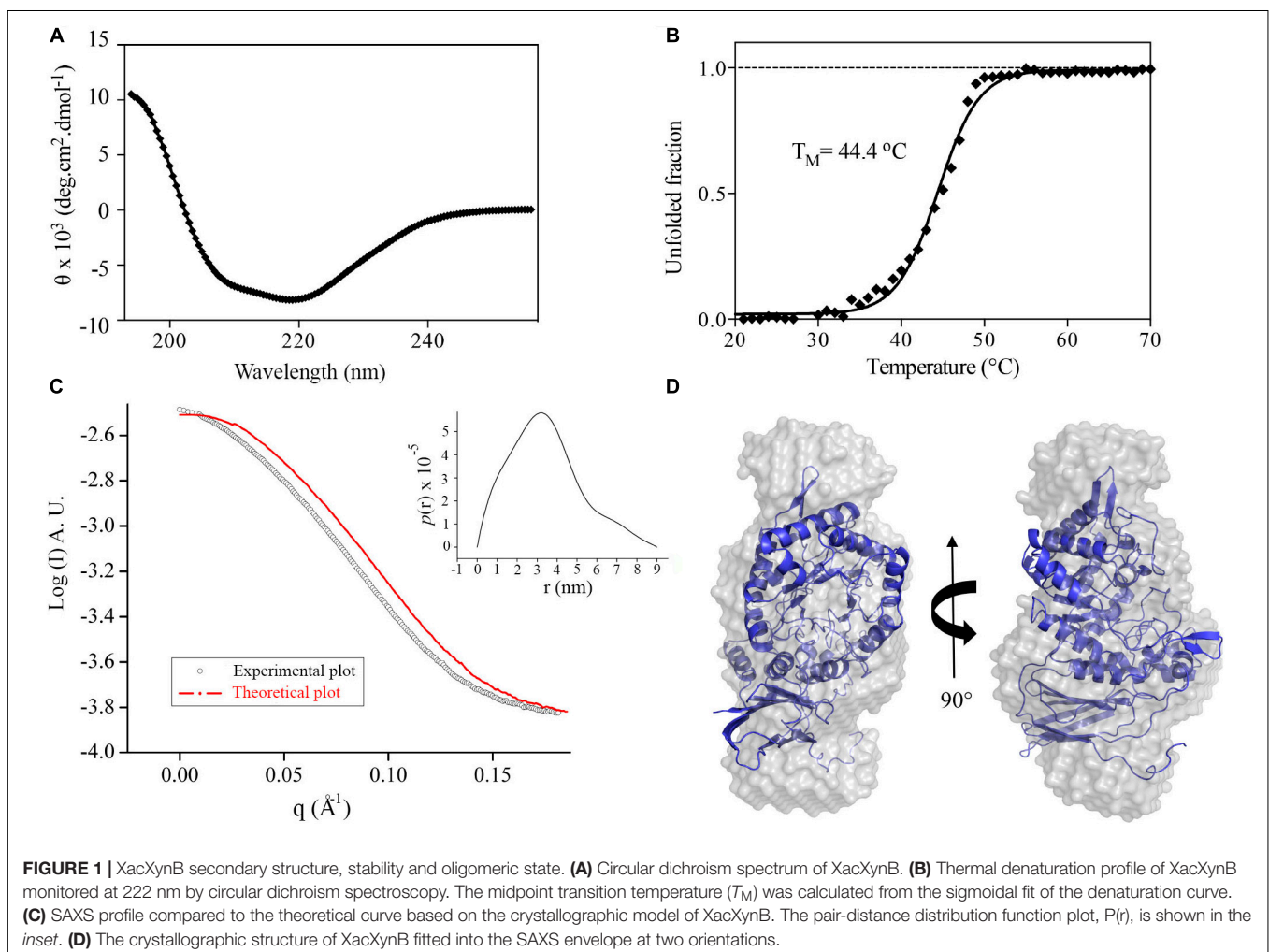
extended to 100 ns (production). Analysis of the trajectories has been carried out using standard tools of AMBER and VMD (Humphrey et al., 1996).

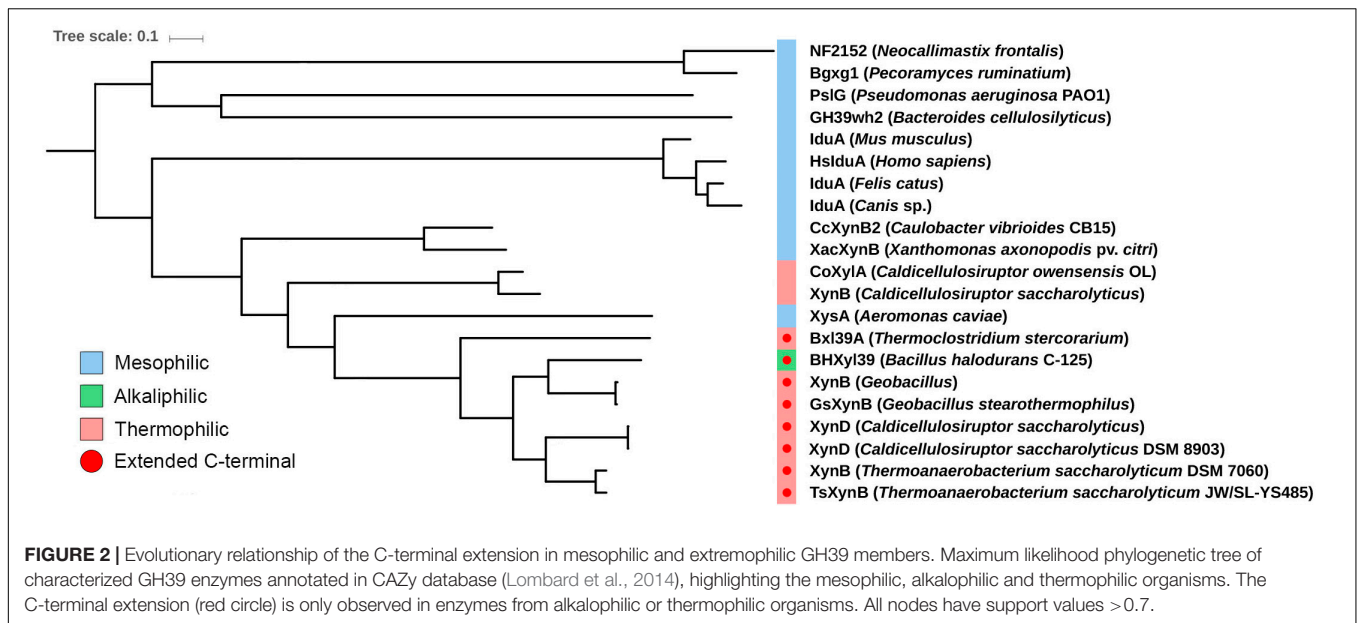
## RESULTS

### C-Terminal Region Affects Oligomerization and Structural Stability

The recombinant GH39 enzyme XacXynB was heterologously expressed in a folded and stable form with a typical CD spectrum of  $\alpha/\beta$  proteins (Figure 1A), which is in accordance with the conserved fold present in GH39  $\beta$ -xylosidases (Yang et al., 2004; Czjzek et al., 2005; Santos et al., 2012). Despite of the modular structural organization with an ancestral accessory domain, the thermal unfolding occurred following a two-state model with a midpoint transition temperature ( $T_M$ ) of 44°C (Figure 1B). This  $T_M$  is similar to that observed for other glycoside hydrolases from *X. citri* (Santos et al., 2014; Domingues et al., 2018).

The oligomeric state of XacXynB in solution was determined by SAXS and resulted in a radius of gyration ( $R_g$ ) of





$2.72 \pm 0.01$  nm. The distance distribution  $[P(r)]$  profile indicates an elongated shape of XacXynB (Figure 1C) with maximum dimensions compatible with a monomeric state. The *ab initio* SAXS modeling resulted in a molecular envelope with a low NSD with the crystallographic monomer (Figure 1D), corroborating the monomeric form of XacXynB in solution. The low-resolution structure and SAXS parameters are similar to those observed for the monomeric GH39 member from *C. crescentus* (CcXynB) (Santos et al., 2012).

Phylogenetic analysis considering all characterized GH39 enzymes available in the CAZy database revealed a correlation between the presence of an extended C-terminus and microorganism extremophilicity (Figure 2 and Supplementary Figure 1). While most GH39 members from extremophilic bacteria contain a C-terminal extension, those adapted to milder conditions systematically lack this motif. It indicates that oligomerization via C-terminal extension might be an important and conserved adaptation in this family to extreme environments.

The XacXynB structure was elucidated at 1.7 Å resolution with one full-length protomer in the asymmetric unit (Table 1). It clearly reveals the lack of C-terminal extension in comparison with thermophilic GH39 structures, from *Thermoanaerobacterium saccharolyticum* (TsXynB) (Yang et al., 2004) and *Geobacillus stearothermophilus* (GsXynB) (Czjzek et al., 2005; Supplementary Figure 2A). In homotetrameric GH39  $\beta$ -xylosidases, the C-terminal extension is swapped between two monomers, forming the main dimer-stabilizing interface, named interface II (Yang et al., 2004; Supplementary Figures 2B,C).

Although the other structural elements (including the dimeric interface I) are conserved in XacXynB, the main dimer-stabilizing interface (type II) is missing due to the lack of the long C-terminus. Crystal packing and energetic analyses by PDBePISA (Krissinel and Henrick, 2007) did not indicate any

energetically stable interface for XacXynB oligomers, supporting the monomeric state observed in solution.

## Active Site Mapping Indicates Room for Accommodation of Xylooligosaccharides With Distinct Degrees of Polymerization

XacXynB conserves canonical elements of GH39 members, with  $(\alpha/\beta)_8$ -barrel catalytic core decorated with two extra  $\beta$ -hairpin motifs (between the secondary elements of the barrel  $\beta_3$ - $\alpha_3$  and  $\beta_6$ - $\alpha_6$ ) and a C-terminal  $\beta$ -sandwich accessory domain with an  $\alpha$ -helical bundle (residues 433–466) (Figure 3A). The ancestral accessory domain is not independent from the catalytic domain being formed additionally by a  $\beta$ -strand from the very N-terminus and tightly associated with the  $\alpha_6$  and  $\alpha_7$  secondary structural elements from the barrel. Similar to CcXynB, XacXynB contains a long  $\alpha$ -helix-containing loop (residues 389–406) between the  $\beta$ -strands 14 and 15 of the accessory domain, which links the accessory domain and the parental catalytic core (Figure 3A). This feature is not observed in any other structurally characterized GH39 members (except CcXynB and XacXynB) conferring a very distinctive catalytic interface. The  $\alpha$ -helical bundle and long  $\alpha$ -helix-containing loop from the accessory domain along with the  $\beta_6$ - $\alpha_6$   $\beta$ -hairpin are critical to stabilize the conformation of loops forming the substrate binding subsites.

Due to crystal packing, the N-terminus of the symmetry molecule is occupying the entire active-site cleft, inserting the side chain of an arginine in the  $-1$  subsite (Figure 3B). This arginine residue (Arg-1) makes part of the synthetically introduced sequence of a 6xHis-tag in the protein and occupied exactly the position of a xylosyl moiety in the  $-1$  subsite interacting with Glu325, Trp317, and Glu279 (Figure 3B). The binding mode of this peptide at the active site along with structural comparisons with the GsXynB complex with 2,5-dinitrophenyl- $\beta$ -D-xyloside allowed to identify putative key

**TABLE 1** | Data collection and refinement statistics of XacXynB.

Data collection	
Space group	C2
<b>Cell dimensions</b>	
a, b, c (Å)	117.14; 57.09; 81.12
$\alpha$ , $\beta$ , $\gamma$ (°)	90; 107.5; 90
Molecules per AU	1
Resolution (Å)	38.67–1.71
Observed reflections	328,998 (29,274)
Unique reflections	54,724 (5,211)
CC <sub>1/2</sub> <sup>†</sup>	0.999 (0.848)
I/ $\sigma$ (I)	20.09 (2.47)
Completeness (%)	98.21 (94.01)
R <sub>meas</sub>	0.058 (0.610)
Multiplicity	6.0 (5.6)
<b>Refinement</b>	
Resolution (Å)	28.93–1.71
Number of reflections	54,710
R <sub>work</sub> /R <sub>free</sub>	0.163/0.197
Number Of protein residues	506
<b>B-factor (Å<sup>2</sup>)</b>	
Average	23.80
Macromolecules	22.80
Solvent	31.26
<b>Root mean square deviations</b>	
Bond lengths (Å)	0.007
Bond angles (°)	1.17
<b>Ramachandran plot</b>	
Favored (%)	98
Allowed (%)	1.8
Disallowed (%)	0.2
Molprobrity clashscore	1.49
Protein Data Bank code	6UJQJ

Values in parentheses are for highest-resolution shell. <sup>†</sup>CC<sub>1/2</sub>: correlation between intensities from random half-datasets (Karplus and Diederichs, 2012).

residues involved in substrate binding such as Phe118, Phe168, Tyr230, Trp317, Glu325, and Phe337 in the  $-1$  subsite and Tyr284 in the  $+1$  subsite, beyond the catalytic residues Glu162 (acid/base) and Glu279 (nucleophile) (Vocadlo et al., 1998; Bravman et al., 2001; Yang et al., 2004; **Figure 3C**). Based on these structural analyses, it would be expected that the active site of XacXynB could accommodate xylooligosaccharides with different degrees of polymerization, which was further confirmed by capillary zone electrophoresis experiments. The enzyme was able to hydrolyze xylooligosaccharides from X2 to X6, producing xylose as the final product (**Figure 4**).

## Positive-Subsite Region Modulates Substrate Affinity

XacXynB showed highest structural similarity with CcXynB among the structurally characterized GH39 members (RMSD = 0.73 Å for all C $\alpha$  atoms). These enzymes strictly conserve the  $-1$  subsite and several other key residues for substrate binding including His61, Phe118, Asn161, Glu162,

Phe168, His228, Tyr230, Glu279, Tyr284, Trp317, Phe323, Glu325, and Phe337 (**Figure 5A**). The exceptions are the residues Lys166 and Asp167, which corresponds to the positive-subsite region (**Figure 5A**). These are preceding the aromatic residue Phe168 directly involved in the recognition of  $-1$  xyloside (**Figure 5A**). The active-site topology is clearly modified by these two residues substitutions compared to CcXynB (**Figures 5B,C**), suggesting that they might play a role in enzyme activity.

Kinetic characterization showed that XacXynB has a fivefold smaller K<sub>M</sub> ( $\sim 1.93$  mM) than CcXynB ( $\sim 9.3$  mM; Corrêa et al., 2012), indicating very distinct substrate affinity among bacterial  $\beta$ -xylosidases from this family. As the only differences observed in the active site of these enzymes are the substitutions K166D and D167G, it would indicate a role of these residues in substrate affinity. Interestingly, the *T. saccharolyticum* GH39  $\beta$ -xylosidase, which also displays a low K<sub>M</sub> (Vocadlo et al., 2002), conserves a lysine (Lys164) and an acidic residue (Glu165) at the corresponding positions of Lys166 and Asp167, supporting their involvement in substrate binding.

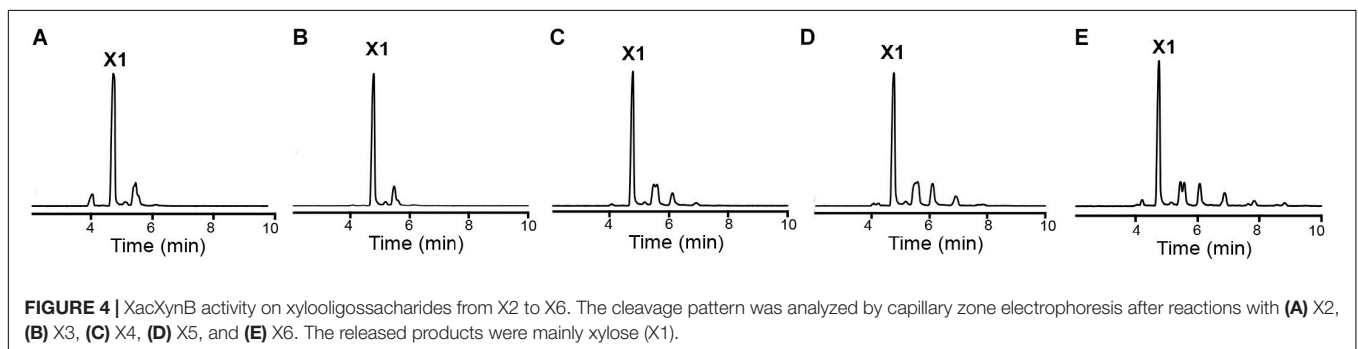
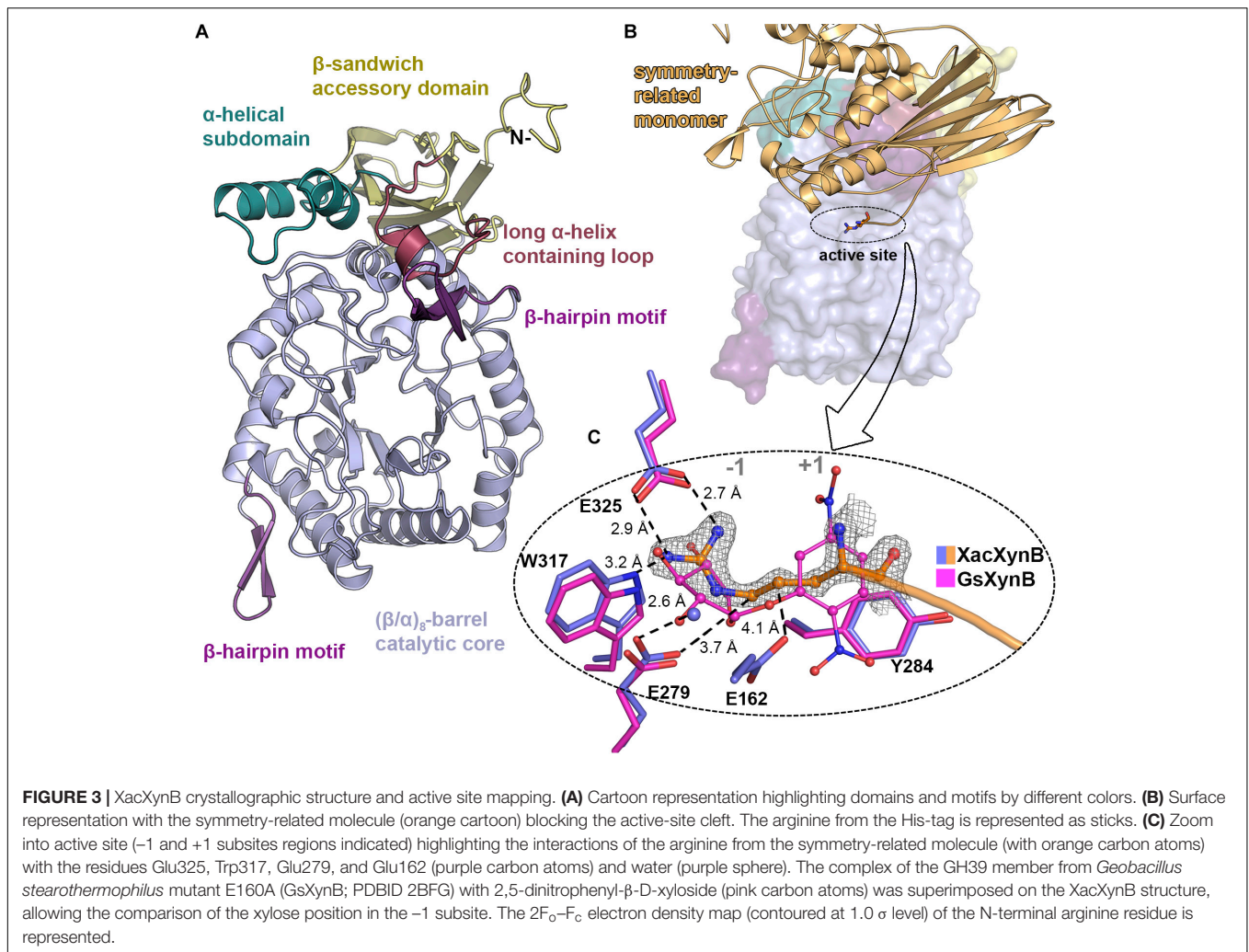
Thus, to experimentally evaluate the role of these residues in substrate affinity, XacXynB Lys166 and Asp167 were mutated to the corresponding residues in CcXynB, an aspartate and a glycine, respectively. These mutations would mimic the GH39  $\beta$ -xylosidase with lower substrate affinity. The pH and temperature dependence for catalytic activity including the k<sub>cat</sub> remained similar to the wild-type enzyme (**Table 2** and **Supplementary Figure 3**). However, both mutants presented higher K<sub>M</sub> values, a twofold increase for the mutant K166D and a threefold increase for the mutant D167G (**Table 2**).

To assess the XacXynB behavior in solution, molecular dynamics simulations were performed with the WT enzyme and with the mutants (K166D and D167G). Global parameters, such as the RMSD, solvent accessible surface area (SASA) and R<sub>g</sub> showed no significant difference between the WT and mutants (**Supplementary Table 1** and **Supplementary Figure 4**), indicating that local changes are responsible for modifying the substrate affinity. SASA and R<sub>g</sub> values were close to the calculated from the crystal structure and obtained experimentally by SAXS, respectively (**Supplementary Table 1**). Root-mean-square fluctuations (RMSF) revealed that the  $\beta$ -hairpin region (residues 231–249) is the most flexible region for both WT and mutants (**Supplementary Figure 4**).

Therefore, these substitutions at the active site have a local effect, possibly affecting the charge distribution and the positive subsite topology, favoring interactions and consequently substrate affinity. Moreover, these residues are preceding Phe168, a critical residue for the binding of the  $-1$  xyloside and a substitution nearby could affect negatively the capacity of the enzyme to interact with the  $-1$  xylosyl moiety.

## DISCUSSION

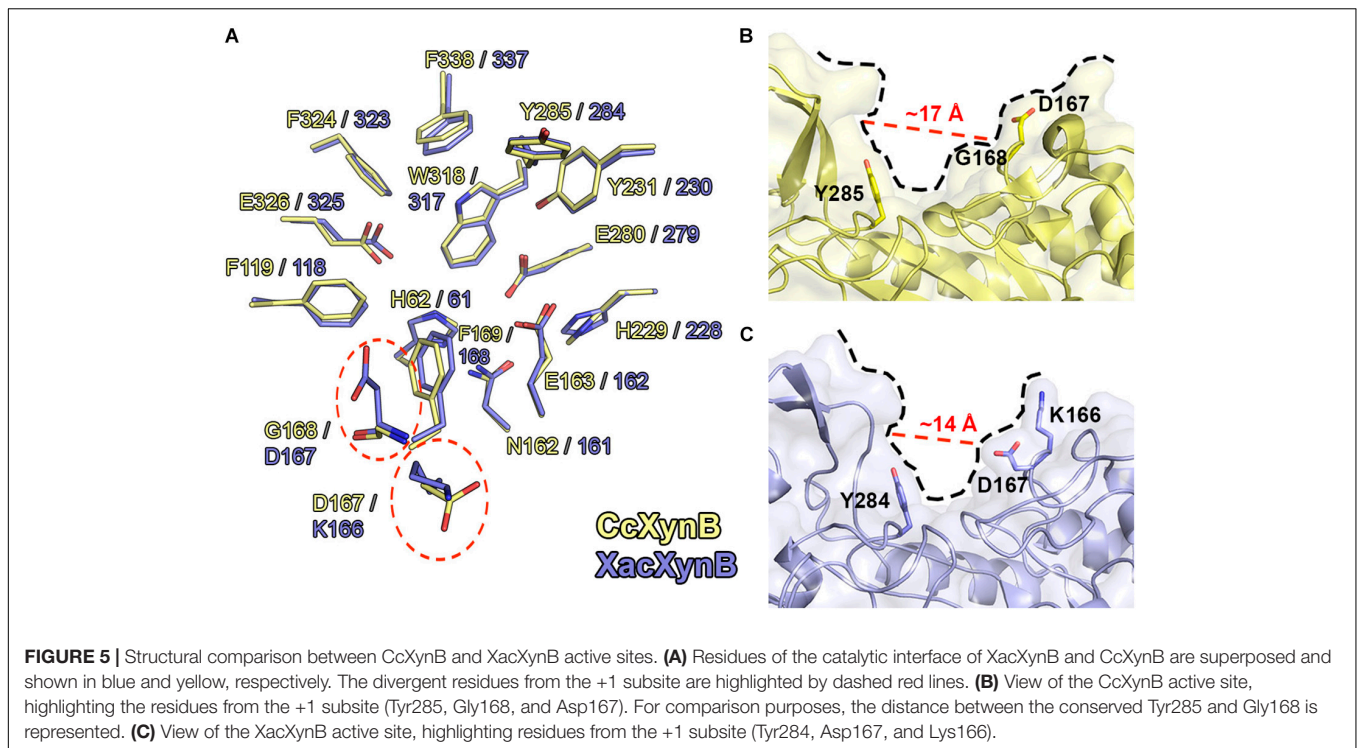
The GH39 family comprises mostly  $\beta$ -xylosidases and  $\alpha$ -iduronidases, with 21 characterized members and only 8 structures (CAZy, Lombard et al., 2014). Recent discoveries of polyspecific GH39 members indicate a functional and structural



diversity in this family. Moreover, these enzymes are found in microorganisms living in various ecological niches including extremophilic environments, raising the interest to understand the molecular adaptations of these enzymes to be active at such harsh conditions. Previous studies suggested an important feature of this family, the C-terminal elongation in extremophilic organisms. Thus, more members of this poorly explored family need to be enzymatically and structurally characterized to validate their functions and oligomerization pattern.

In this work, a new GH39 enzyme was investigated, contributing to elucidate the structural basis for substrate affinity and to expand the concept of oligomerization as a conserved molecular strategy to gain of stability in bacterial GH39  $\beta$ -xylosidases.

XacXynB is a mesophilic  $\beta$ -xylosidase that, like CcXynB, features a shortened C-terminus that directly implicates in the oligomerization of these proteins. Both behave as monomers in solution, whereas GH39 members from extremophilic organisms,



TsXynB and GsXynB, contain the C-terminal region extended and form tetramers in solution (Yang et al., 2004; Czjzek et al., 2005). The C-terminal extension is involved in the largest contact interface that leads to oligomerization being essential for this process. Correlation between these features indicates the oligomerization as a conserved strategy in the GH39 family to enhance structural stability. By phylogenetic analysis, we verified that only GH39 from extremophilic organisms contain the C-terminal extension. Curiously, two enzymes from thermophilic species (*Caldicellulosiruptor* sp.) do not have an extended C-terminus. However, biophysical data showed that GH39 CoXylA (from *Caldicellulosiruptor owensensis*) forms dimers in solution (Mi et al., 2014), yet supporting oligomerization as an adaptive strategy for extreme environments. It is likely that in the genus *Caldicellulosiruptor* other molecular mechanisms were evolved for oligomerization and gain of stability; however, the lack of high-resolution structural data does not currently allow us to precisely predict how it occurs.

The use of oligomerization to adapt to extreme environments or to change enzyme activity is not a distinguishing characteristic of GH39 family and other CAZy families also make use of this strategy such as GH1 (Zanphorlin et al., 2016), GH5

(Lafond et al., 2016), GH10 (Santos et al., 2014), and GH32 (Sainz-Polo et al., 2013).

The unexpected occupation of the catalytic interface of XacXynB by a peptide segment from the N-terminal Histag revealed conserved interactions with sugars moieties based on structural superpositions with other GH39  $\beta$ -xylosidases in complex with xylose and analogs. According to these analyses, XacXynB active site might be able to accommodate substrates with distinct degrees of polymerization as previously observed in a GH39 member with enlarged active-site pocket (Czjzek et al., 2005). Using the capillary electrophoresis we verified the xylose release from different XOS from X2 to X6 demonstrating the capacity of XacXynB to cleave such substrates. It represents an interesting feature for industrial applications involving lignocellulose saccharification, since XOS larger than X2 that are released during hemicellulose cleavage, might competitively inhibit cellulases (Qing et al., 2010).

In addition, structural comparative analysis with CcXynB allowed the identification of non-conserved residues at the positive-subsite region that could be relevant for catalytic activity of GH39  $\beta$ -xylosidases. By site-directed mutagenesis and molecular dynamics simulations, we revealed that the residues Lys166 and Asp167 in XacXynB can promote a gain in the substrate affinity without interfering in other catalytic properties or structural elements. These residues locally change the charge and topology of the active-site pocket, possibly increasing the interactions at the positive-subsite region with the substrate and stabilize the aromatic residue Phe168 involved in the interaction with -1 xyloside.

Together, our results demonstrate the importance of oligomerization in bacterial GH39  $\beta$ -xylosidases adaptation to

**TABLE 2 |** Kinetic parameters of the wild-type XacXynB and the mutants K166D and D167G on 4-nitrophenyl  $\beta$ -D-xylopyranoside.

	$K_M$ (mM)	$k_{cat}$ ( $\text{min}^{-1}$ )	$k_{cat}/K_M$ ( $\text{min}^{-1} \text{mM}^{-1}$ )
WT	$1.93 \pm 0.25$	$266.0 \pm 8.5$	137.8
K166D	$4.06 \pm 0.39$	$219.2 \pm 6.8$	54.0
D167G	$5.79 \pm 0.35$	$281.0 \pm 6.2$	48.5

extreme environments and how the positive-subsite region might be redesigned to modulate substrate affinity, furthering in the mechanistic understanding of this CAZy family.

## ACCESSION NUMBERS

Atomic coordinates and structure factors have been deposited in the Protein Data Bank under accession code 6UQJ.

## DATA AVAILABILITY STATEMENT

The datasets generated for this study are available on request to the corresponding author.

## AUTHOR CONTRIBUTIONS

MAM, CP, and MM designed the study, performed simulations, structural analysis, and wrote the manuscript. MAM, CP, MD, RP, FS, and JC performed the cloning, protein expression and purification, and, biochemical and biophysical experiments. GP made phylogenetic analysis and figures. MAM, CP, and CS crystallized the protein and solved the crystal and SAXS structures. All authors analyzed the results and, read and approved the final manuscript.

## REFERENCES

- Afonine, P. V., Grosse-Kunstleve, R. W., Echols, N., Headd, J. J., Moriarty, N. W., Mustyakimov, M., et al. (2012). Towards automated crystallographic structure refinement with phenix refine. *Acta Cryst. D Biol. Crystallogr.* 68, 352–367. doi: 10.1107/S0907444912001308
- Ali-Ahmad, A., Garron, M. L., Zamboni, V., Lefant, N., Nurizzo, D., Henrissat, B., et al. (2017). Structural insights into a family 39 glycoside hydrolase from the gut symbiont *Bacteroides cellulosilyticus* WH2. *J. Struct. Biol.* 197, 227–235. doi: 10.1016/j.jsb.2016.11.004
- Baker, P., Whitfield, G. B., Hill, P. J., Little, D. J., Pestrak, M. J., Robinson, H., et al. (2015). Characterization of the *Pseudomonas aeruginosa* glycoside hydrolase PslG reveals that its levels are critical for psl polysaccharide biosynthesis and biofilm formation. *J. Biol. Chem.* 290, 28374–28387. doi: 10.1074/jbc.M115.674929
- Bravman, T., Mechaly, A., Shulami, S., Belakhov, V., Baasov, T., Shoham, G., et al. (2001). Glutamic acid 160 is the acid base catalyst of b-xylosidase from *Bacillus stearothermophilus* T-6: a family 39 glycoside hydrolase. *FEBS Lett.* 495, 115–119. doi: 10.1016/s0014-5793(01)02371-7
- Case, D. A., Ben-Shalom, I. Y., Brozell, S. R., Cerutti, D. S., Cheatham, T. E. III, Cruzeiro, V. W. D., et al. (2018). *AMBER 2018*. San Francisco, CA: University of California.
- Chen, V. B., Arendall, W. B. III, Headd, J. J., Keedy, D. A., Immormino, R. M., Kapral, G. J., et al. (2010). MolProbity: all-atom structure validation for macromolecular crystallography. *Acta Cryst. D Biol. Crystallogr.* 66, 12–21. doi: 10.1107/S0907444909042073
- Corrêa, J. M., Graciano, L., Abrahão, J., Loth, E. A., Gandra, R. F., Kadowaki, M. K., et al. (2012). Expression and characterization of a GH39  $\beta$ -Xylosidase II from *Caulobacter crescentus*. *Appl. Biochem. Biotechnol.* 168, 2218–2229. doi: 10.1007/s12010-012-9931-1
- Czjzek, M., David, A. B., Bravman, T., Shoham, G., Henrissat, B., and Shoham, Y. (2005). Enzyme-substrate complex structures of a GH39  $\beta$ -Xylosidase from *Geobacillus stearothermophilus*. *J. Mol. Biol.* 353, 838–846. doi: 10.1016/j.jmb.2005.09.003

## FUNDING

This work was supported by the São Paulo Research Foundation (grant numbers #2015/26982-0, #2016/19995-0, and #2013/24622-0).

## ACKNOWLEDGMENTS

We are thankful to the Brazilian Synchrotron Light Laboratory (LNLS-CNPEM/MCTIC) for the provision of time on the MX2 and SAXS1 beamlines. We also thank the Brazilian Biosciences National Laboratory (LNBio-CNPEM/MCTIC) for the use of ROBO LAB and the Brazilian Biorenewables National Laboratory (LNBR-CNPEM/MCTIC) during the use of the Characterization of Macromolecules (MAC) open-access facility. We also thank the Barcelona Supercomputing Center (BSC) and Prof. Carme Rovira for support with MD simulations.

## SUPPLEMENTARY MATERIAL

The Supplementary Material for this article can be found online at: <https://www.frontiersin.org/articles/10.3389/fbioe.2020.00419/full#supplementary-material>

- Déjean, G., Blanvillain-Baufume, S., Boulanger, A., Darrasse, A., Dugede Bernonville, T., Girard, A. L., et al. (2013). The xylan utilization system of the plant pathogen *Xanthomonas campestris* pv. *campestris* controls epiphytic life and reveals common features with oligotrophic bacteria and animal gut symbionts. *New Phytol.* 198, 899–915. doi: 10.1111/nph.12187
- Domingues, M. N., Souza, F. H. M., Vieira, P. S., Morais, M. A. B., Zanphorlin, L. M., Santos, C. R., et al. (2018). Structural basis of exo-beta-mannanase activity in theGH2 family. *J. Biol. Chem.* 293, 13636–13649. doi: 10.1074/jbc.RA118.002374
- Emsley, P., and Cowtan, K. (2004). Coot: model-building tools for molecular graphics. *Acta Cryst. D Biol. Crystallogr.* 60, 2126–2132. doi: 10.1107/S0907444910007493
- Hammersley, A. P., Brown, K., Burmeister, W., Claustre, L., Gonzalez, A., McSweeney, S., et al. (1997). Calibration and application of an X-ray image intensifier/ charge-coupled device detector for monochromatic macromolecular crystallography. *J. Synch. Rad.* 4, 67–77. doi: 10.1107/S0909049596015087
- Humphrey, W., Dalke, A., and Schulten, K. (1996). VMD: visual molecular dynamics. *J. Mol. Graph.* 14, 33–38.
- Jones, D. R., Uddin, M. S., Gruninger, R. J., Pham, T. T. M., Thomas, D., Boraston, A. B., et al. (2017). Discovery and characterization of family 39 glycoside hydrolases from rumen anaerobic fungi with polyspecific activity on rare arabinosyl substrates. *J. Biol. Chem.* 292, 12606–12620. doi: 10.1074/jbc.M117.789008
- Jorgensen, W. L., Chandrasekhar, J., Madura, J. D., Impey, R. W., and Klein, M. L. (1983). Comparison of simple potential functions for simulating liquid water. *J. Chem. Phys.* 79, 926–935.
- Kabsch, W. (2010). XDS. *Acta Cryst. D Biol. Crystallogr.* 66, 125–132. doi: 10.1107/S0907444909047337
- Karplus, P. A., and Diederichs, K. (2012). Linking crystallographic model and data quality. *Science* 336, 1030–1033. doi: 10.1126/science.1218231
- Katoh, K., Misawa, K., Kuma, K., and Miyata, T. (2002). MAFFT: a novel method for rapid multiple sequence alignment based on fast Fourier transform. *Nucleic Acids Res.* 30, 3059–3066. doi: 10.1093/nar/gkf436

- Kozin, M., and Svergun, D. (2001). Automated matching of high- and low-resolution structural models. *J. Appl. Cryst.* 34, 33–41. doi: 10.1107/S0021889800014126
- Krissinel, E., and Henrick, K. (2007). Inference of macromolecular assemblies from crystalline state. *J. Mol. Biol.* 372, 774–797. doi: 10.1016/j.jmb.2007.05.022
- Lafond, M., Sulzenbache, G., Freyd, T., Henrissat, B., Berrin, J. G., and Garron, M. L. (2016). The quaternary structure of a glycoside hydrolase dictates specificity toward  $\beta$ -Glucans\*. *J. Biol. Chem.* 291, 7183–7194. doi: 10.1074/jbc.M115.695999
- Li, H., Robertson, A. D., and Jensen, J. H. (2005). Very fast empirical prediction and rationalization of protein pKa values. *Proteins* 61, 704–721. doi: 10.1002/prot.20660
- Lombard, V., Golaconda Ramulu, H., Drula, E., Coutinho, P. M., and Henrissat, B. (2014). The carbohydrate-active enzymes database (CAZy) in 2013. *Nucleic Acids Res.* 42, D490–D495. doi: 10.1093/nar/gkt1178
- Maier, J. A., Martinez, C., Kasavajhala, K., Wickstrom, L., Hauser, K. E., and Simmerling, C. (2015). ff14SB: improving the accuracy of protein side chain and backbone parameters from ff99SB. *J. Chem. Theory Comp.* 11, 3696–3713. doi: 10.1021/acs.jctc.5b00255
- McCoy, A. J., Grosse-Kunstleve, R. W., Adams, P. D., Winn, M. D., Storoni, L. C., and Read, R. J. (2007). Phaser crystallographic software. *J. Appl. Cryst.* 40, 658–674. doi: 10.1107/S0021889807021206
- McIlvaine, T. C. (1921). A buffer solution for colorimetric comparison. *J. Biol. Chem.* 49, 183–186.
- Mi, S., Jia, X., Wang, J., Qiao, W., Peng, X., and Han, Y. (2014). Biochemical characterization of two thermostable xylanolytic enzymes encoded by a gene cluster of *Caldicellulosiruptor owensensis*. *PLoS One* 9:e105264. doi: 10.1371/journal.pone.0105264
- Murshudov, G. N., Vagin, A. A., and Dodson, E. J. (1997). Refinement of macromolecular structures by the maximum-likelihood method. *Acta Cryst. D Biol Crystallogr.* 53, 240–255. doi: 10.1107/S0907444996012255
- Price, M. N., Dehal, P. S., and Arkin, A. P. (2010). FastTree 2 - Approximately maximum-likelihood trees for large alignments. *PLoS One* 5:e9490. doi: 10.1371/journal.pone.0009490
- Qing, Q., Yang, B., and Wyman, C. E. (2010). Xylooligomers are strong inhibitors of cellulose hydrolysis by enzymes. *Bioresour. Technol.* 101, 9624–9630. doi: 10.1016/j.biortech.2010.06.137
- Rajeshwari, R., Jha, G., and Sonti, R. V. (2005). Role of an in planta-expressed xylanase of *Xanthomonas oryzae* pv. *oryzae* in promoting virulence on rice. *Mol. Plant. Microbe Interact.* 18, 830–837. doi: 10.1094/MPMI-18-0830
- Ryckaert, J. P., Ciccotti, G., and Berendsen, H. J. C. (1977). Numerical integration of the cartesian equations of motion of a system with constraints: molecular dynamics of n-alkanes. *J. Comput. Phys.* 23, 327–341.
- Sainz-Polo, M. A., Ramírez-Escudero, M., Lafraya, A., González, B., Marín-Navarro, J., Polaina, J., et al. (2013). Three-dimensional structure of saccharomyces invertase. *J. Biol. Chem.* 288, 9755–9766. doi: 10.1074/jbc.M112.446435
- Santos, C. R., Hoffmam, Z. B., de Matos Martins, V. P., Zanphorlin, L. M., de Paula Assis, L. H., Honorato, R. V., et al. (2014). Molecular mechanisms associated with xylan degradation by *Xanthomonas* plant pathogens. *J. Biol. Chem.* 289, 32186–32200. doi: 10.1074/jbc.M114.605105
- Santos, C. R., Polo, C. C., Corrêa, J. M., Simão, R. C. G., Seixas, F. A. V., and Murakami, M. T. (2012). The accessory domain changes the accessibility and molecular topography of the catalytic interface in monomeric GH39  $\beta$ -xylosidases. *Acta Cryst. D Biol Crystallogr.* 68, 1339–1345. doi: 10.1107/S0907444912028491
- Silva, A. C., Ferro, J. A., Reinach, F. C., Farah, C. S., Furlan, L. R., Quaggio, R. B., et al. (2002). Comparison of the genomes of two *Xanthomonas* pathogens with differing host specificities. *Nature* 417, 459–463. doi: 10.1038/417459a
- Svergun, D. I. (1992). Determination of the regularization parameter in indirect-transform methods using perceptual criteria. *J. Appl. Cryst.* 25, 495–503. doi: 10.1107/S0021889892001663
- Svergun, D. I. (1999). Restoring low resolution structure of biological macromolecules from solution scattering using simulated annealing. *Biophys. J.* 76, 2879–2886. doi: 10.1016/S0006-3495(99)77443-6
- Szczesny, R., Jordan, M., Schramm, C., Schulz, S., Coge, V., Bonas, U., et al. (2010). Functional characterization of the Xcs and Xps type II secretion systems from the plant pathogenic bacterium *Xanthomonas campestris* pv. *vesicatoria*. *New Phytol.* 187, 983–1002. doi: 10.1111/j.1469-8137.2010.03312.x
- Vocadlo, D. J., MacKenzie, L. F., He, S., Zeikus, G. J., and Withers, S. G. (1998). Identification of glu-277 as the catalytic nucleophile of *Thermoanaerobacterium saccharolyticum*  $\beta$ -xylosidase using electrospray MS. *Biochem. J.* 335, 449–455. doi: 10.1042/bj3350449
- Vocadlo, D. J., Wicki, J., Rupitz, K., and Withers, S. G. (2002). Mechanism of *Thermoanaerobacterium saccharolyticum*  $\beta$ -xylosidase: kinetic studies. *Biochemistry* 41, 9727–9735. doi: 10.1021/bi020077v
- Volkov, V. V., and Svergun, D. I. (2003). Uniqueness of ab initio shape determination in small-angle scattering. *J. Appl. Cryst.* 36, 860–864. doi: 10.1107/S0021889803000268
- Yang, J. K., Yoon, H. J., Ahn, H. J., Lee, B. II, Pedelacq, J. D., Liang, E. C., et al. (2004). Crystal structure of  $\beta$ -D-Xylosidase from *Thermoanaerobacterium saccharolyticum*, a family 39 glycoside hydrolase. *J. Mol. Biol.* 335, 155–165. doi: 10.1016/j.jmb.2003.10.026
- Zanphorlin, L. M., de Giuseppe, P. O., Honorato, R. V., Tonoli, C. C., Fattori, J., Crespim, E., et al. (2016). Oligomerization as a strategy for cold adaptation: structure and dynamics of the GH1  $\beta$ -glucosidase from *Exiguobacterium antarcticum* B7. *Sci. Rep.* 31:23776. doi: 10.1038/srep23776

**Conflict of Interest:** The authors declare that the research was conducted in the absence of any commercial or financial relationships that could be construed as a potential conflict of interest.

Copyright © 2020 Morais, Polo, Domingues, Persinoti, Pirolla, de Souza, Correa, dos Santos and Murakami. This is an open-access article distributed under the terms of the Creative Commons Attribution License (CC BY). The use, distribution or reproduction in other forums is permitted, provided the original author(s) and the copyright owner(s) are credited and that the original publication in this journal is cited, in accordance with accepted academic practice. No use, distribution or reproduction is permitted which does not comply with these terms.